Analysis of optical gyroscopes with vertically stacked ring resonators

Dooyoung HAH[*]

Electrical & Electronics Engineering Department, Faculty of Engineering, Abdullah Gül University, Kayseri, Turkey

Abstract: Without any moving part, optical gyroscopes exhibit superior reliability and accuracy in comparison to mechanical sensors. Microring-resonator-based optical gyroscopes emerged as alternatives for bulky conventional Sagnac interferometer sensors, especially attractive for applications with limited footprints. Previously, it has been reported that planar incorporation of multiple resonators does not bring about improvement in sensitivity for a given area because the increase in Sagnac phase accumulation does not outrun the increase of area. Therefore, it was naturally suggested to consider vertical stacking of ring resonators because then, the resonators can share the same footprint. In this work, sensitivity performances of such configurations with vertically stacked microring resonators are analyzed and compared to that of a basic (single-resonator) configuration. Through comprehensive study, it is learned that the sensitivity performance of the devices with vertically-stacked resonators (either with a single bus waveguide or with two bus waveguides) does not exceed that of the basic sensor device (single resonator with one bus waveguide), i.e. the basic structure is yet to be remained as the most efficient configuration.

Key words: Angular rate sensor, gyroscope, optical sensor, ring resonator

1. Introduction

Angular rate sensors, also called as gyroscopes, are essential components for various applications including inertial navigation systems, stability control systems, health monitoring, consumer electronics (e.g. cell phones and remote game controllers), and so on. In comparison to mechanical angular rate sensors which exploit either conservation of angular momentum or Coriolis force, optical counterparts are advantageous in the following aspects. First, they do not suffer from mechanical drift or friction owing to absence of moving parts. Second, they exhibit better reliability for the same reason. Finally, they have minimal interaxial crosstalk because of negligible coupling between orthogonal constituents. Almost all of the optical gyroscopes rely on the Sagnac effect, which is based on invariance of the speed of light in all inertial frames of reference [1]. The conventional optical gyroscopes are realized as a Sagnac interferometer [2]. In this configuration, light is split into two, rotates around an optical loop in opposite directions (either in free space or in an optical fiber), and exits the ring while undergoing interference. Rotation of the frame of reference induces a phase difference between the counter-rotating lights. The incurred phase difference (ϕ_{Sagnac}) is proportional to the inner product of the area ($\vec{A}$) of the loop and the angular velocity ($\vec{\Omega}$) that the frame of reference experiences, as expressed by the

---

[*]Correspondence: dooyoung.hah@agu.edu.tr

following equation [3].

$$\phi_{Sagnac} = \frac{2\omega}{c^2} \left(\vec{A} \cdot \vec{\Omega} \right),$$ (1)

where ω and c are the angular frequency of the light and the speed of light in free space, respectively.

Recent development in photonic integrated circuit (PIC) technologies introduced various new types of sensors [4], including gyroscopes. Utilizing nano-/micro-optical devices such as photonic crystals [5, 6], microring resonators [7–25], and microsphere resonators [26], this new type of sensors can be lighter, more compact and scalable, compared to the bulky conventional ones which are implemented either by free-space optics or by fiber optics. Among the PIC implementations, the sensors based on microring resonators drew particular attention of many researchers. Various configurations have been studied (mostly theoretically) for optical gyroscopes, including coupled resonator optical waveguides (CROW) [7–17], side-coupled integrated spaced sequence of optical resonators (SCISSOR) [18], self-interference add-drop resonators (SIDAR) [19], add-drop multiplexers [20], double-ring resonators [21, 22], and Mach–Zehnder interferometer [23]. The main operation principle of the ring-resonator-based optical gyroscopes can be described as the accumulation of the Sagnac phase (ϕ_{Sagnac}) while light is rotating around the ring multiple times.

Most of the configurations studied so far for the ring-resonator optical gyroscopes have been implemented in a single layer. In the meantime, many configurations in the literature include multiple resonators in order to increase the Sagnac phase accumulation. However, this results in increased footprint, which makes it disadvantageous in terms of a sensitivity for a given area, an important figure of merit. Therefore, it is natural to propose vertical stacking of multiple resonators because addition of more resonators does not increase the footprint proportionally, if not at all. In this paper, optical gyroscopes with vertically stacked ring resonators will be studied and compared to the basic configuration with a single-level implementation, especially in terms of maximum sensitivity. Two different configurations will be included in the study. Section 2 will present analysis of an optical gyroscope with a single bus waveguide and two ring resonators. In Section 3, a sensor with two bus waveguides and two ring resonators will be investigated. Finally, the paper will be concluded in Section 4.

2. Single bus waveguide configuration

Figure 1 illustrates the conceptual sketch of the optical gyroscope with the single-bus-waveguide/two-resonator configuration with vertical stacking. Light that enters the bus waveguide is coupled to the bottom resonator (coupling region 1), which is at the same level as the bus waveguide on top of a lower cladding layer. While propagating inside the bottom resonator, light, then, is coupled to the top resonator vertically, in the area where the two resonators are overlapped (coupling region 2). Two resonators are separated by a middle cladding layer. There can be an optional upper cladding layer on top of the top resonator and the middle cladding layer, but omitted in the sketch for simplicity. A part of the light that is coupled to the resonators, is eventually coupled back to the bus waveguide and exits from the output.

The radii of the two resonators (R_{br} for the bottom resonator and R_{tr} for the top resonator) can be different for extra degree of freedom, and the coupling coefficients for two coupling regions are to be adjusted independently. The coupling coefficients can be determined by adjusting the gap between the waveguides. Figure 2 presents an example of calculated coupling coefficients as a function of the gap between a bus waveguide and a ring resonator. The coefficients were calculated with a two-dimensional finite-difference time-domain (FDTD) method by using Rsoft's FullWAVE$^{\text{TM}}$ (version 2016.09). A snapshot from the simulation is also
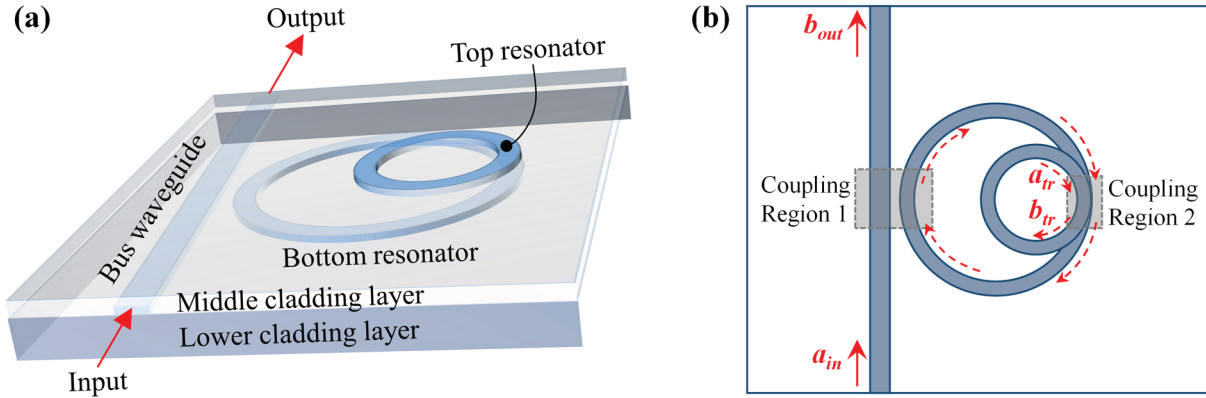
Figure 1. Conceptual sketches of the single-bus-waveguide/two-resonator optical gyroscope. (a) Bird's eye view, and (b) top view. a_{in}, b_{out}, a_{tr} and b_{tr} are optical fields. Two resonators are vertically stacked. Red arrows indicate the direction of the light propagation. Coupling occurs horizontally in the region 1 between the bus waveguide and the bottom resonator, while it occurs vertically in the region 2 between the two resonators. A substrate is omitted underneath the lower cladding layer in the sketch for simplicity.

shown in Figure 2. Only the coupling region was considered in the simulation due to the large size of the resonator while the entrances and the exits were modelled with the PEC (perfect electrical conductor) boundary conditions. Extremely small coupling is expected outside the coupling region. Parameters used in the simulation are summarized in Table 1. Silicon oxynitride and silicon dioxide were considered as a core and a cladding, respectively [27]. With the chosen materials and the core width (1 μm), the waveguide supports a single mode. It can be observed that the coupling coefficient increases as the gap narrows, reaching a maximum with the gap around 1.17 μm. When the gap is further reduced, the coupling coefficient oscillates due to return of the coupled light.

Table 1. Simulation parameters.

Description	Value	Description	Value
Core refractive index	1.50	Core width	1 μm
Cladding refractive index	1.46	Resonator radius	5 cm

The input-output relationship between a_{in} and b_{out} can be established as follows, by using a coupling matrix formalism that was introduced by Poon et al [28].

$$b_{out} = \frac{t_1 \left(1 - t_2 e^{-j\phi_{tr}}\right) - \left(t_2 - e^{-j\phi_{tr}}\right) e^{-j2\phi_{br}}}{1 - t_2 e^{-j\phi_{tr}} - t_1 t_2 e^{-j2\phi_{br}} + t_1 e^{-j(2\phi_{br}+\phi_{tr})}} a_{in}, \tag{2}$$

, where κ_i and t_i, assumed to be real numbers, are coupling and transmission coefficients, respectively, which satisfy $\kappa_i^2 + t_i^2 = 1$ for lossless coupling. The index i is '1' for the coupling between the bus waveguide and the bottom resonator (coupling region 1), and '2' for between the resonators (coupling region 2). ϕ_{br} and ϕ_{tr} are the phase change for a half of the roundtrip around the bottom resonator, and that for a full roundtrip around the top resonator, respectively. These phases are the summation of the pure propagation term (ϕ_{bias}),
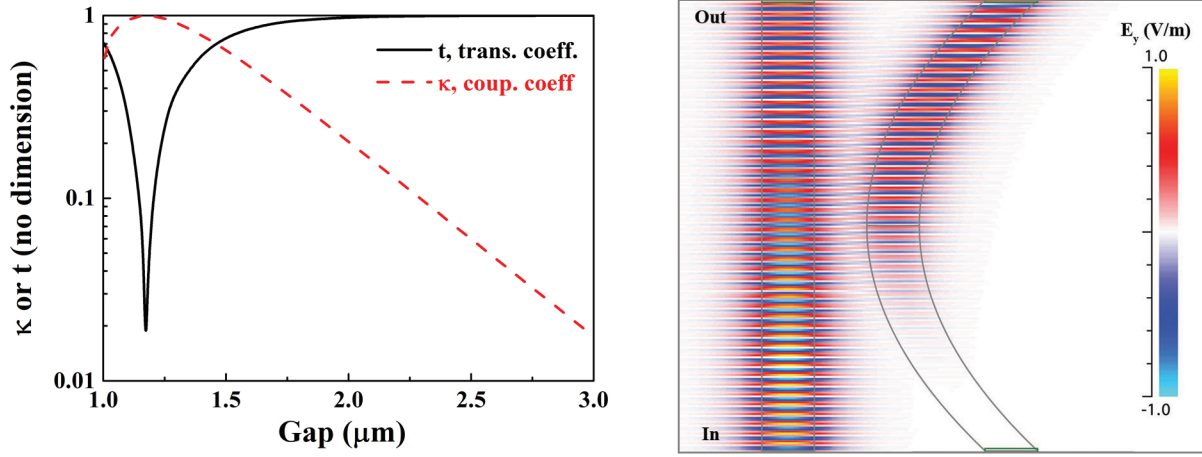
Figure 2. (Left) coupling (κ; red, dashed) and transmission (t; black, solid) coefficients between a bus waveguide and a ring resonator (radius: 5 cm) as a function of a gap between them, calculated by two-dimensional FDTD simulation. Simulation parameters are summarized in Table 1. (Right) a snapshot from a FDTD simulation, showing electric field (E_y). Gray outlines indicate the bus waveguide and a part of the ring resonator. Light coupling from the bus waveguide to the resonator part is clearly observed. Waveguide widths: 1 μm. Only the coupling region is considered. Radius of the ring resonator: 1 mm. Input polarization: TE. Wavelength: 700 nm.

the Sagnac effect term (ϕ_{Sagnac}), and the loss term (ϕ_{loss}), as follows.

$$\phi_{br} = \phi_{bias,br} + \phi_{Sagnac,br} + \phi_{loss,br} = \frac{\pi R_{br} n_{ring} \omega}{c} + \frac{\pi R_{br}^2 \Omega \omega}{c^2} - j\frac{\pi R_{br}\alpha}{2}, \tag{3}$$

$$\phi_{tr} = \phi_{bias,tr} + \phi_{Sagnac,tr} + \phi_{loss,tr} = \frac{2\pi R_{tr} n_{ring} \omega}{c} + \frac{2\pi R_{tr}^2 \Omega \omega}{c^2} - j\pi R_{tr}\alpha. \tag{4}$$

, where n_{ring} and α are the effective index of the ring resonator and the loss coefficient, respectively. $\phi_{bias,br}$ and $\phi_{bias,tr}$ are the design parameters, which can be chosen to maximize the sensitivity of the sensor. These bias phases can be adjusted by slightly changing the resonator radii. In (3) and (4), it is assumed that the rotation axis of the frame of reference is parallel to the normal direction of the sensor plane. The sensitivity (S) of the device is defined as

$$S = \frac{1}{P_0}\frac{dP}{d\Omega}, \tag{5}$$

where P_0 and P are the input and output powers, respectively.

Figure 3 shows an example of the output power (P) versus angular velocity (Ω), calculated by using (2)–(4). MATLAB® was used for the calculation in this work, but other programming languages can be used for the same results. The graph shows a dip in the output power near zero angular velocity, which is desirable to result in high sensitivity around it. More precisely, it is advantageous to place the zero velocity at the steepest slope of the curve for high sensitivity. This can be achieved by selecting the coupling coefficients and the phase biases adequately.

Figure 4(a) presents the calculated sensitivities by using (2)-(5), for different values of κ_1 and κ_2, while optimal $\phi_{bias,br}$ and $\phi_{bias,tr}$ values are sought and used for each pair of the coupling coefficients. Sensitivity

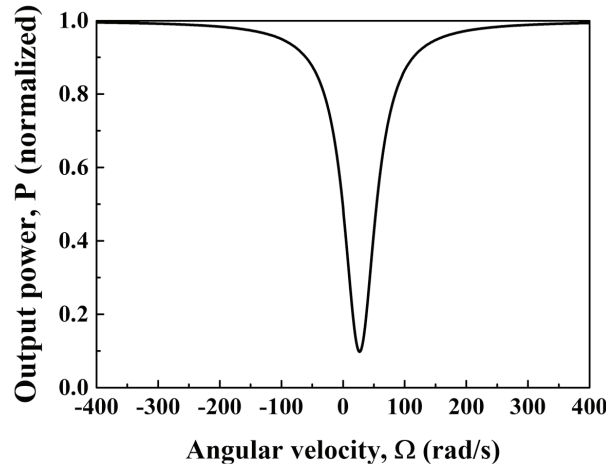**Figure 3**. Calculated output power (P, normalized) as a function of the angular velocity (Ω). Wavelength (λ) = 700 nm, R_{br} = 5 cm, R_{tr} = 3.54 cm, α = 0.06 m^{-1}, κ_1 = 0.1, κ_2 = 0.06, $\phi_{bias,br}$ = 3.14 rad, and $\phi_{bias,tr}$ = 0.37 rad.

was calculated at zero angular velocity. R_{tr} was chosen to be $R_{br}/\sqrt{2}$ so that the top resonator has the half the area of the bottom resonator. It can be seen that the sensitivity is high around κ_1 value of 0.1. The maximum sensitivity is found to be 0.0191 Hz^{-1} when κ_1 = 0.1, κ_2 = 0.06, $\phi_{bias,br}$ = 3.139 rad, and $\phi_{bias,tr}$ = 1.436 rad. Figure 4(b) exhibits the effect of ϕ_{bias} values to the sensitivity at the optimal coupling coefficient values. It can be seen that $\phi_{bias,br}$ has the greater influence to the sensitivity than $\phi_{bias,tr}$.
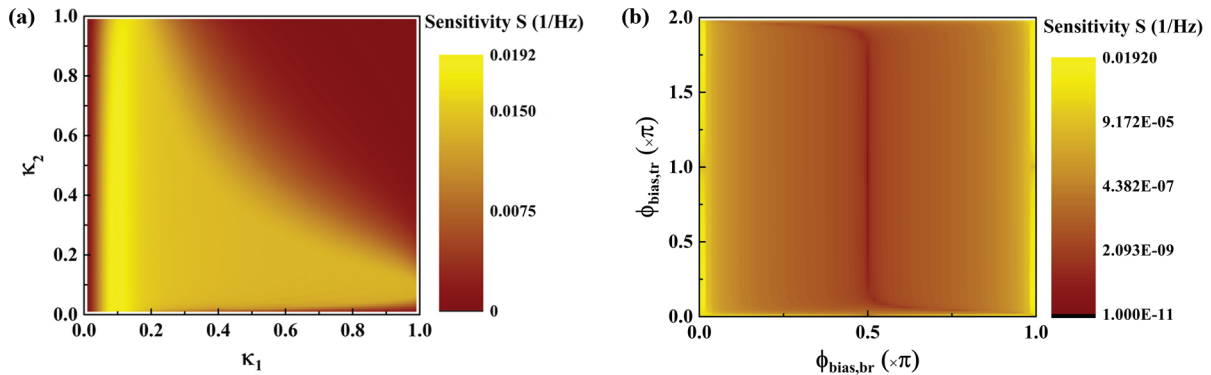

Figure 4. Calculated sensitivities as a function of (a) κ_1 and κ_2 when optimal $\phi_{bias,br}$ and $\phi_{bias,tr}$ values are used for each pair of κ_1 and κ_2, and (b) $\phi_{bias,br}$ and $\phi_{bias,tr}$ when κ_1 = 0.1 and κ_2 = 0.06. λ = 700 nm, R_{br} = 5 cm, R_{tr} = 3.54 cm, α = 0.06 m^{-1}. Color maps: (a) linear scale, (b) logarithmic scale.

Terrel et al. reported that the maximum sensitivity (S_{RFOG}) of a single-bus-waveguide/single-resonator gyroscope [8] is a function of the ring radius (R), the frequency of the light (ω), and the loss coefficient (α), and they derived it as follows:

$$S_{RFOG} = \frac{4R\omega}{3\sqrt{3}\alpha c^2}.$$

(6)

If the value of R_{br} (the larger of the two radii, i.e. 5 cm) is used in (6), S_{RFOG} is calculated as 0.0192 Hz^{-1},

which is almost the same as that of the current device with two resonators. Since the two devices have the same footprint, it can be concluded that they have the same sensitivity per area. In order to delve into the matter further, the maximum sensitivity was calculated for different combinations of the ring radii values as presented in Figure 5(a). The result indicates that the maximum sensitivity is determined by the larger of the two radii. It is also found that the maximum sensitivity is almost equal to the value given in (6) when the larger radius of the two is used as R. It should be noted that the similar configuration but on a single level should result in the equivalent sensitivity. Therefore, the vertical-stack configuration can have up to two times higher sensitivity per area in comparison to a single-level configuration with two resonators.
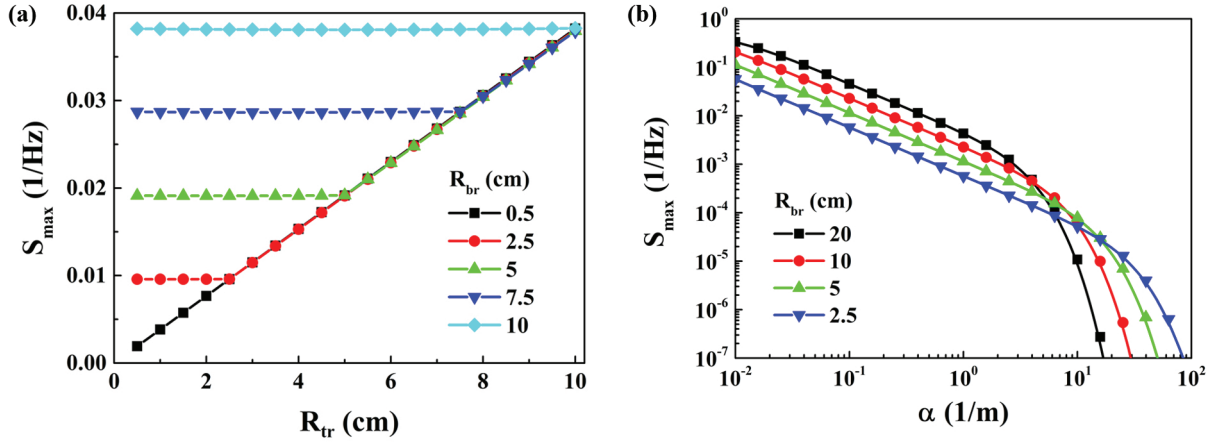

Figure 5. Calculated maximum sensitivities (S_{max}) as a function of (a) R_{br} and R_{tr} when $\alpha = 0.06$ m^{-1}, and (b) R_{br} and α when $R_{tr} = R_{br}/\sqrt{2}$. $\lambda = 700$ nm. For each data point, the optimal values of κ_1, κ_2, $\phi_{bias,br}$, and $\phi_{bias,tr}$ were found and used.

(6) indicates that the maximum sensitivity is inversely proportional to α, the loss coefficient. [8] also states that (6) is valid for a small value of $\pi R \alpha$. In order to examine this point in depth, the maximum sensitivities were calculated for different values of α and R_{br}, while the value of R_{tr} was set as $R_{br}/\sqrt{2}$ (see Figure 5b). The result shows that (6) is valid for small $\pi R \alpha$ values indeed, and the maximum sensitivity starts to deviate from (6) at around $\pi R \alpha \approx 1$. It is also shown that the larger the R_{br} value is, the more rapidly the maximum sensitivity value declines from the value estimated by (6).

3. Two bus waveguide configuration

Figure 6 depicts the conceptual sketch of the optical gyroscope with two bus waveguides and two ring resonators. This configuration is often used as an add-drop multiplexer, and hence, the input/output field components for the second waveguide are named as a_{add} and b_{drop}. The second bus waveguide is laid at the same level as the top resonator. Therefore, coupling between the bus waveguide 2 and the top resonator occurs horizontally (coupling region 3). In this configuration, the output can be taken from the out port, from the drop port, or as the combination of the two. From the sketch, it can be understood that there are two overlapping regions between the bus waveguide 2 and the bottom resonator, and hence, vertical coupling can occur here. However, since the waveguide is very narrow (in the order of μm), such a coupling is considered to be negligible, and hence will be ignored in the analysis.

By using the same derivation method, and by setting $a_{in} = 1$ and $a_{add} = 0$, the input/output relationships
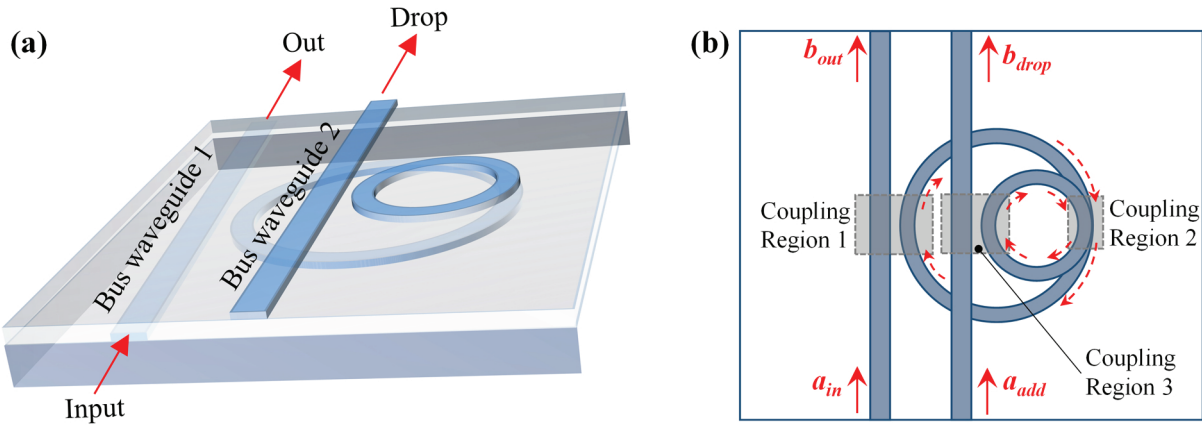
Figure 6. Conceptual sketches of the two-bus-waveguide/two-resonator optical gyroscope. (a) Bird's eye view, and (b) top view. a_{in}, b_{out}, a_{add} and b_{drop} are optical fields.

can be found as:

$$b_{out} = \frac{2t_1 \cos(\phi_{br} + \phi_{tr}) - 2t_2 \cos(\phi_{br} - \phi_{tr}) + \kappa_1^2 t_2 e^{j(\phi_{br} - \phi_{tr})}}{2 \cos(\phi_{br} + \phi_{tr}) - 2t_1 t_2 \cos(\phi_{br} - \phi_{tr}) - \kappa_1^2 e^{-j(\phi_{br} + \phi_{tr})}}. \tag{7}$$

$$b_{drop} = \frac{-\kappa_1^2 \kappa_2}{2 \cos(\phi_{br} + \phi_{tr}) - 2t_1 t_2 \cos(\phi_{br} - \phi_{tr}) - \kappa_1^2 e^{-j(\phi_{br} + \phi_{tr})}}. \tag{8}$$

In (7) and (8), it is assumed that the bus waveguide/resonator coupling coefficients (i.e. at the coupling regions 1 and 3) are the same for the both regions. ϕ_{tr} in (7) and (8) is different from that of (2) because it is redefined as a phase change for a half of the round trip.

Figure 7 presents the calculated maximum sensitivities for different coupling coefficient values and for the three different output scenarios aforementioned. For the combined output scenario, it was considered that the each output (from the out and the drop ports) is converted to voltage first by photodetectors, and then, added together as voltages. It is found out that the sensitivity is much higher when the output is taken from the out port ($S_{max} = 0.0191$ Hz^{-1}), in comparison to when it is taken just from the drop port ($S_{max} = 0.0049$ Hz^{-1}). Moreover, the combined case shows negligible improvement in terms of the sensitivity ($S_{max} = 0.0192$ Hz^{-1}) when compared to the out port only case. This occurs because the optimal coupling coefficient and bias phase values do not coincide exactly between the out port and the drop port, and hence the combination cannot be realized in a strongly constructive manner. Overall, the maximum sensitivity obtained is almost the same as that of the single-bus-waveguide configuration of Section 2. Therefore, it can be concluded that adding the second bus waveguide does not bring benefit to the device performance.

Figure 8 shows the effect of ϕ_{bias} values to the sensitivity for each of the output scenarios with the optimal coupling coefficient values for each scenario. High sensitivities are found with ϕ_{bias} values around 0 or π. Figure 9 shows the effect of the top resonator radius (R_{tr}) to the maximum sensitivity (S_{max}) when the bottom resonator radius (R_{br}) is fixed as 5 cm. When R_{tr} is smaller than R_{br}, the results are similar to the one presented in Figures 7 and 8, with minimal change in the sensitivity for the out port only case as well as the combined case, and slight increase for the drop port only case, as R_{tr} increases. However, when R_{tr} is larger
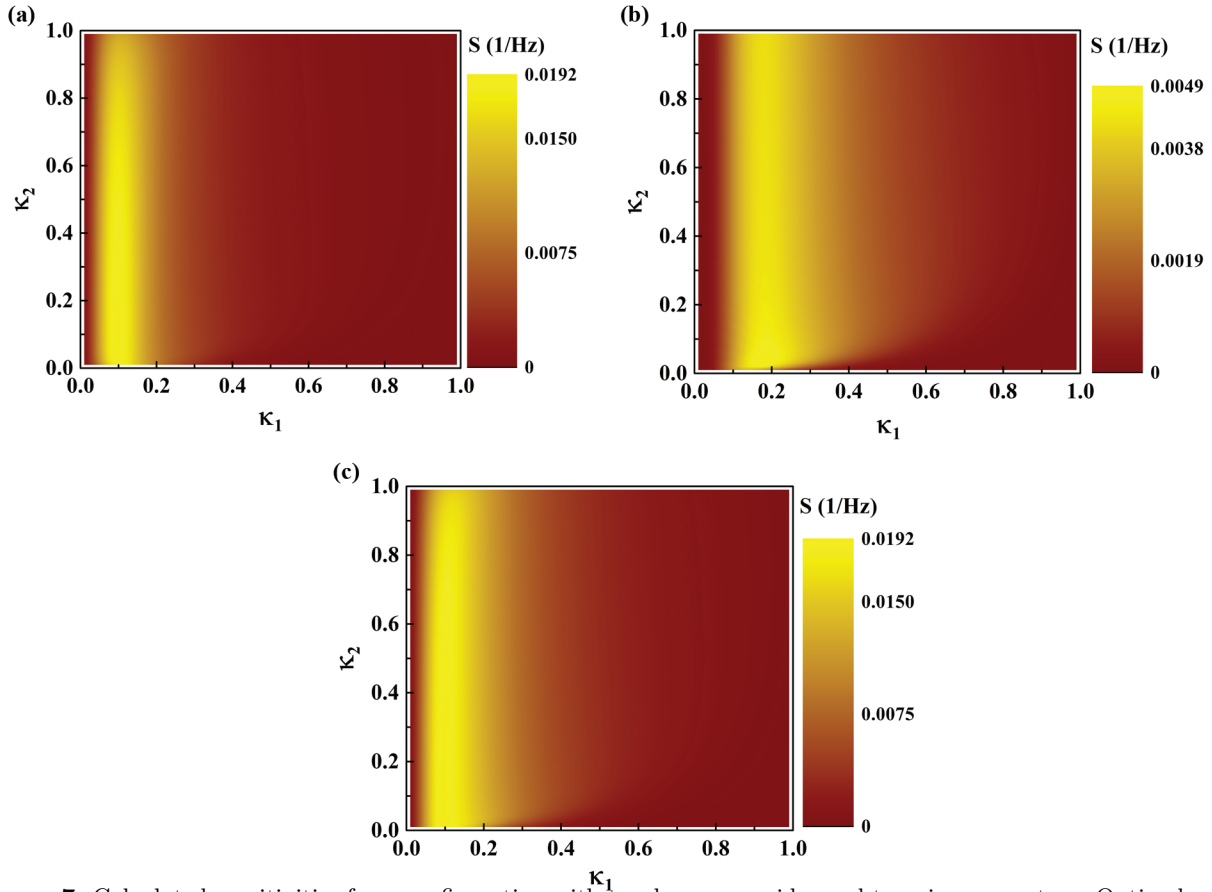
Figure 7. Calculated sensitivities for a configuration with two bus waveguides and two ring resonators. Optimal values of ϕ_{bias} values were found and used for each pair of coupling coefficients. Output is taken (a) from the out port, (b) from the drop port, and (c) as a combination. $R_{br} = 5$ cm, $R_{tr} = 3.54$ cm, $\lambda = 700$ nm, $\alpha = 0.06$ m^{-1}. Optimal values of κ_1, κ_2, $\phi_{bias,br}$, and $\phi_{fbias,tr}$ are found to be 0.1, 0.09, 0.006 rad, 0.772 rad for (a), 0.18, 0.03, 0.018 rad, 0.018 rad for (b), and 0.1, 0.07, 0.003 rad, and 2.271 rad for (c), respectively. Color maps: linear scale.

than R_{br}, the result becomes substantially different. The combined case produces considerably higher S_{max} than the out port only case, but at the same time, cannot reach the value calculated by (6), i.e. S_{RFOG}. For example, when R_{tr} is 10 cm and R_{br} is 5 cm, S_{max} values are 0.0232 Hz^{-1} (Out port), 0.009 Hz^{-1} (Drop port), 0.0276 Hz^{-1} (combined), and 0.0384 Hz^{-1} (S_{RFOG}). It is interesting to note that the sensitivity results change completely when the values of R_{br} and R_{tr} are swapped. When R_{br} is 10 cm and R_{tr} is 5 cm, S_{max} values become 0.038 Hz^{-1} (Out port), 0.009 Hz^{-1} (Drop port), 0.0382 Hz^{-1} (combined), and 0.0384 Hz^{-1} (S_{RFOG}), again S_{max} almost reaching the limit of S_{RFOG}. Therefore, it can be concluded that for the higher sensitivity for a two-bus-waveguide/two-resonator device, it is necessary to have the bottom resonator bigger than the top resonator, rather than the other way around.

4. Conclusion

Optical gyroscopes with vertically stacked ring resonators were analyzed and presented. Effect of ring radii, a loss coefficient, coupling coefficients, and ring bias phases to the sensor sensitivity were studied. The configuration was proposed with the rationale of increasing the Sagnac phase accumulation without increasing the footprint. Through comprehensive analysis, it was shown that the proposed vertical-stack configuration can have up to two
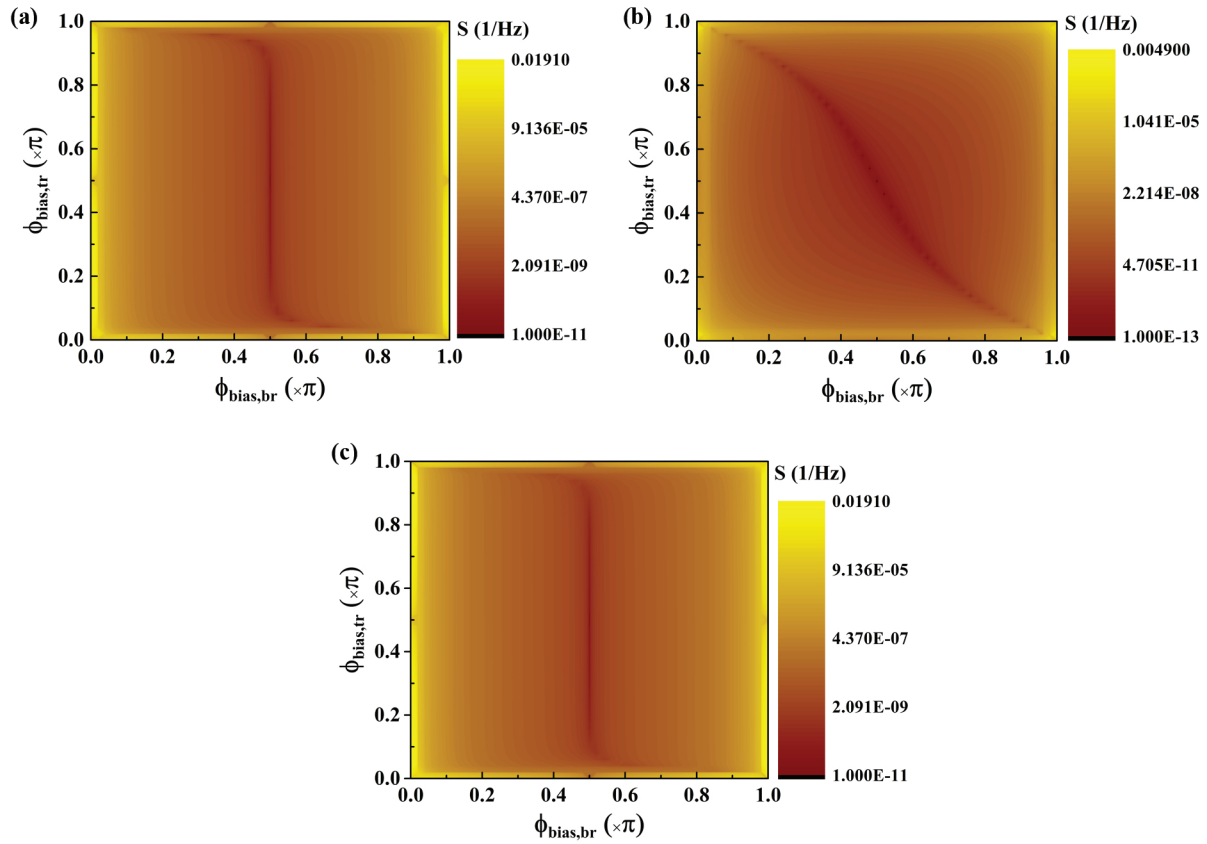
Figure 8. Calculated sensitivities for different values of $\phi_{bias,br}$ and $\phi_{bias,tr}$ for a configuration with two bus waveguides and two ring resonators. (a) Output is taken from the Out port, $\kappa_1 = 0.1$, $\kappa_2 = 0.09$. (b) Output is taken from the drop port, $\kappa_1 = 0.18$, $\kappa_2 = 0.03$. (c) Output is taken as a combination, $\kappa_1 = 0.1$, $\kappa_2 = 0.07$. $\lambda = 700$ nm, $R_{br} = 5$ cm, $R_{tr} = 3.54$ cm, $\alpha = 0.06$ m^{-1}. Color maps: logarithmic scale.
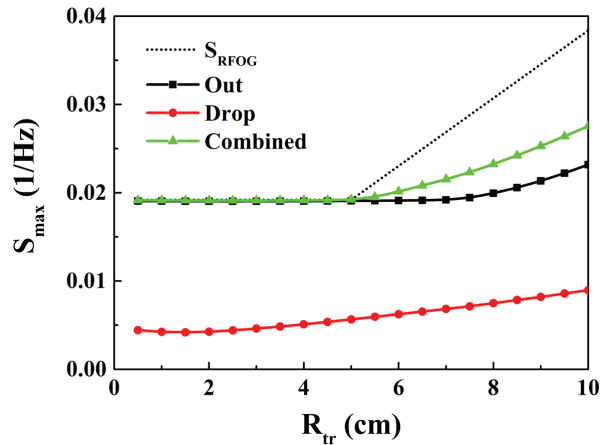

Figure 9. Calculated maximum sensitivities (S_{max}) as a function of R_{tr} for different output scenarios: Out port only (black square), drop port only (red circles), and combined output (green triangles). S_{RFOG} calculated with (6) is plotted as a dashed line. $R_{br} = 5$ cm, $\lambda = 700$ nm, $\alpha = 0.06$ m^{-1}. For each data point, the optimal values of κ_1, κ_2, $\phi_{bias,br}$, and $\phi_{bias,tr}$ were found and used.

times higher sensitivity per area when compared to the single-level configuration with the same number of ring resonators. It also turned out that the maximum sensitivity of the proposed devices either with single or two bus waveguides do not exceed that of the single bus waveguide/one resonator device of the same footprint. The reason behind these results is deemed that the increased loss by incorporating multiple resonators undermines the gain in accumulated Sagnac phase.

It should be noted that research efforts in this topic has been mainly focused on the search of the configuration with improved performance, especially in terms of sensitivity. It is anticipated that once the optimum configuration is determined, investigation on other performance aspects such as bandwidth, linearity, dynamic range, and so on will be commenced.

References

[1] Post EJ. Sagnac effect. Review of Modern Physics 1967; 39 (2): 475-493. doi: 10.1103/RevModPhys.39.475

[2] Bergh RA, Lefevre HC, Shaw HJ. An overview of fiber-optic gyroscopes. Journal of Lightwave Technology 1984; 2 (2): 91-107. doi: 10.1109/JLT.1984.1073580

[3] Hurst RB, Wells JPR, Stedman GE. An elementary proof of the geometrical dependence of the Sagnac effect. Journal of Optics A: Pure and Applied Optics 2007; 9: 838-841. doi: 10.1088/1464-4258/9/10/010

[4] Arafin S, Coldren LA. Advanced InP photonic integrated circuits for communication and sensing. Journal of Selected Topics in Quantum Electronics 2018; 24 (1): 6100612. doi: 10.1109/JSTQE.2017.2754583

[5] Steinberg BZ. Rotating photonic crystals: A medium for compact optical gyroscopes. Physical Review E 2005; 71: 056621. doi: 10.1103/PhysRevE.71.056621

[6] Steinberg BZ, Scheuer J, Boag A. Rotation-induced superstructure in slow-light waveguides with mode-degeneracy: optical gyroscopes with exponential sensitivity. Journal of Optical Society of America B 2007; 24 (5): 1216-1224. doi: 10.1364/JOSAB.24.001216

[7] Scheuer J, A Yariv. Sagnac effect in coupled-resonator slow-light waveguide structures. Physical Review Letters 2006; 96: 053901. doi: 10.1103/PhysRevLett.96.053901

[8] Terrel M, Digonnet MJF, Fan S. Performance comparison of slow-light coupled-resonator optical gyroscopes. Laser & Photonics Reivews 2009; 3 (5): 452-465. doi: 10.1002/lpor.200810052

[9] Gad M, Yevick D, Jessop P. High sensitivity ring resonator gyroscopes. Fiber and Integrated Optics 2011; 30 (6): 395-410. doi: 10.1080/01468030.2011.611581

[10] Novitski R, Steinberg BZ, Scheuer J. Losses in rotating degenerate cavities and a coupled-resonator optical-waveguide rotation sensor. Physical Review A 2012; 85: 023813. doi: 10.1103/PhysRevA.85.023813

[11] Kalantarov D, Search C. Effect of input–output coupling on the sensitivity of coupled resonator optical waveguide gyroscopes. Journal of Optical Society of America B 2013; 30 (2): 377-381. doi: 10.1364/JOSAB.30.000377

[12] Kalantarov D, Search C. Effect of resonator losses on the sensitivity of coupled resonator optical waveguide gyroscopes. Optics Letters 2014; 39 (4): 985-988. doi: 10.1364/OL.39.000985

[13] Toland JRE, Search CP. Sagnac gyroscope using a two-dimensional array of coupled optical microresonators. Applied Physics B 2014; 114: 333-339. doi: 10.1007/s00340-013-5520-4

[14] Novitski R, Steinberg BZ, Scheuer J. Finite-difference time-domain study of modulated and disordered coupled resonator optical waveguide rotation sensors. Optics Express 2014; 22 (19): 23153. doi: 10.1364/OE.22.023153

[15] Kalantarov D, Search C. Sensitivity limits of coupled resonator optical waveguide (CROW) gyroscopes when subject to material losses. Gyroscopy and Navigation 2015; 6 (1): 33-40. doi: 10.1134/S2075108715010058

[16] Aghaie KZ, Vigneron PB, Digonnet MJF. Rotation sensitivity analysis of a two-dimensional array of coupled resonators. In: Proceedings of SPIE OPTO; San Francisco, California, USA; 2015. doi: 10.1117/12.2086775

[17] Scheuer J. Quantum and thermal noise limits of coupled resonator optical waveguide and resonant waveguide optical rotation sensors. Journal of Optical Society of America B 2016; 33 (9): 1827-1835. doi: doi.org/10.1364/JOSAB.33.001827

[18] Matsko AB, Savchenkov AA, Ilchenko VS, Maleki L. Optical gyroscope with whispering gallery mode optical cavities. Optics Communications 2004; 233: 107-122. doi: 10.1016/j.optcom.2004.01.035

[19] Tian H, Zhang Y. Rotation sensing based on the Sagnac effect in the self-interference add–drop resonator. Journal of Lightwave Technology 2018; 36 (10): 1792-1797. doi: 10.1109/JLT.2017.2788499

[20] Hah D, Zhang D. Analysis of resonant optical gyroscopes with two input/output waveguides. Optics Express 2010; 18 (17): 18200-18205. doi: 10.1364/OE.18.018200

[21] Gu H, Liu X. Study of double-ring slow-light gyroscope with two input–output waveguides. Optics Communications 2017; 400: 96-100. doi: 10.1016/j.optcom.2017.04.066

[22] Grant MJ, Digonnet MJF. Double-ring resonator optical gyroscopes. Journal of Lightwave Technology 2018; 36 (13): 2708-2715. doi: 10.1109/JLT.2018.2818754

[23] Zhang H, Chen J, Jin J, Lin J, Zhao L et al. On-chip modulation for rotating sensing of gyroscope based on ring resonator coupled with Mach-Zehnder interferometer. Scientific Reports 2018; 6: 19024. doi: 10.1038/srep19024

[24] Peng C, Li Z, Xu A. Rotation sensing based on a slow-light resonating structure with high group dispersion. Applied Optics 2007; 46 (19): 4125-4131. doi: 10.1364/AO.46.004125

[25] Peng C, Li Z, Xu A. Optical gyroscope based on a coupled resonator with the all-optical analogous property of electromagnetically induced transparency. Optics Express 2007; 15 (7): 3864-3875. doi: 10.1364/OE.15.003864

[26] An P, Zheng Y, Yan S, Xue C, Wang W et al. High-Q microsphere resonators for angular velocity sensing in gyroscopes. Applied Physics Letters 2015; 106: 063504. doi: 10.1063/1.4908053

[27] Kijaszek W, Oleszkiewicz W, Zakrzewski A, Patela S, Tlaczala M. Investigation of optical properties of silicon oxynitride films deposited by RF PECVD method. Materials Science-Poland 2016; 34 (4): 868-871. doi: 10.1515/msp-2016-0111

[28] Poon JKS, Scheuer J, Mookherjea S, Paloczi GT, Huang Y et al. Matrix analysis of microring coupled-resonator optical waveguides. Optics Express 2004; 12 (1): 90-103. doi: 10.1364/OPEX.12.000090